Hindawi
Journal of Nanomaterials
Volume 2019, Article ID 6368789, 11 pages
https://doi.org/10.1155/2019/6368789

Research Article

Ultrasonic-Assisted Synthesis, Characterization, and Photocatalytic Application of SiO_2@TiO_2 Core-Shell Nanocomposite Particles

Newaz Mohammed Bahadur,[1,2] **Farhana Chowdhury**,[2] **Md. Obaidullah**,[3] **Md. Shahadat Hossain**,[2] **Rumana Rashid**,[4] **Yeasmin Akter**,[2] **Takeshi Furusawa**,[1] **Masahide Sato**,[1] **and Noboru Suzuki**[1,3]

[1]*Department of Material and Environmental Chemistry, Graduate School of Engineering, Utsunomiya University, Yoto 7-1-2, Utsunomiya 321-8585, Japan*
[2]*Department of Applied Chemistry and Chemical Engineering, Noakhali Science and Technology University, Noakhali 3814, Bangladesh*
[3]*Department of Innovation Systems Engineering, Utsunomiya University, Yoto 7-1-2, Utsunomiya 321-8585, Japan*
[4]*Department of Public Health Nutrition, Primeasia University, Banani, Dhaka, Bangladesh*

Correspondence should be addressed to Newaz Mohammed Bahadur; nmbahadur@yahoo.com

Received 9 February 2019; Revised 11 July 2019; Accepted 23 July 2019; Published 10 September 2019

Academic Editor: Hiromasa Nishikiori

In this study, we report the synthesis of SiO_2@TiO_2 core-shell nanocomposite particles by ultrasound irradiation of a mixture of dispersed SiO_2 nanoparticles, titanium-tetra-n-butoxide (TBOT), and ammonia in an ethanol-water solution medium. The resulting core-shell nanocomposite particles were characterized by SEM, TEM, FT-IR, XPS, XRF, zeta potential measurements, XRD, and UV-visible spectroscopy. Results showed that TiO_2 nanoparticles coated on the surface of SiO_2 were 6–10 nm in size and retained an anatase crystalline phase. Zeta potential measurements confirmed that the surface property of the SiO_2 changed after TiO_2 coating. SiO_2@TiO_2 core-shell particles demonstrated better decolorization of methylene blue dye compared to commercial TiO_2 in aqueous solution under UV light. After treatment, the catalysts were separated with low-speed centrifugation and successfully reused four times without loss of activity. This study may provide some inspiration for the synthesis of other metal oxide-metal oxide core-shell nanocomposite materials through ultrasound irradiation.

1. Introduction

The boom in industrialization and mass production undoubtedly benefit humans with numerous latest products and services. However, different industries such as textile, paper, leather, ceramic, cosmetics, and ink and food processing release various organic and inorganic pollutants, which cause a great health hazard to humans and the aquatic environment when discharged to the environment without further treatment [1]. Among the pollutants, synthetic organic dyes used as coloring agents are considered as one of the potential sources of nonaesthetic pollutants which contaminate surface and ground water and can harm ecological resources including water quality, soils, plants, and animals and also human health [2, 3]. A number of technologies have been developed to remove the organic pollutants including chemical treatment such as chlorination [3] and ozonation [4], electrochemical treatment [5], physical treatment such as adsorption by activated carbon [6] and membranes [7], biological treatment, and a combined chemical-biological method [8]. Although the biological method is cost-effective, the dyes are only adsorbed on the sludge and are not degraded in this method [9]. Physical methods also have the disadvantages such as the pollutants simply transfer from

one phase to another rather than their destruction. It has been found that photocatalysis is a promising technique for the destruction of dyes using semiconductor catalysts under light irradiation [10]. In addition, as per literature reports, enough research work has also been carried out related to the purification of water by photocatalysis [11]. Various types of photocatalysts such as TiO_2, ZnO, Al_2O_3, WO_3, Fe_3O_4, CeO_2, and their composites have been used for the degradation of organic pollutants [12]. Among these metal oxides, titanium dioxide (TiO_2) has attracted much attention due to its wide range of applications such as paint industry, biomedicine, electronics, and environmental engineering [13]. TiO_2 has also been widely used as the photocatalyst because of its chemical and biological inertness, high stability against photocorrosion, nontoxicity, low cost, and excellent degradation for organic pollutants [2, 13, 14].

Despite the favorable properties of TiO_2 in the decomposition of dyes, it is not thermally stable when applied independently as a powder form and tends to dissolve with losing its surface area in the solution. It is also known that when TiO_2 nanoparticle is used as free-suspending systems in photocatalysis, it shows better efficiency and photocatalytic activity compared to the encapsulated ones [15–17]. However, there are a number of disadvantages of using free-suspending systems such as loss of catalyst, instability of the catalyst particles, and difficulties for the separation of the particles after treatment. Nevertheless, one of the major drawbacks of TiO_2 photocatalyst is the low quantum efficiency of TiO_2 owing to the fast recombination of photogenerated electron-hole pairs, which significantly reduces the photocatalytic activity of TiO_2. Therefore, the low photocatalytic efficiency of the TiO_2 photocatalyst still remained a challenge and is insufficient for industrial-scaled applications. In order to minimize the above drawbacks, TiO_2 is incorporated in high surface area materials. Incorporation comprises an increase in the surface area of TiO_2, controlling the crystalline phase of TiO_2 as anatase even at high-temperature treatment to increase its crystallinity. In addition, composites made from TiO_2 and other metal oxides were often used to improve the photocatalytic activity of TiO_2 [18]. Among various types of metal oxides, SiO_2 has drawn large interest due to its chemical inertness and stability at high temperature [19, 20]. Incorporation of TiO_2 in silica has many advantages including easy separation of the nanocomposites by low-speed centrifugation when the size of the carrier spheres (SiO_2) is large but small enough for easy dispersion in the system. Besides, silica is a cost-effective support possessing good mechanical strength for long-time operations compared to polymer-based carriers. Moreover, the encapsulation of TiO_2 on high surface adsorbent silica spheres significantly facilitates reactant molecules to reach the active sites of TiO_2. Therefore, the photocatalytic activity increases [18, 19]. SiO_2 traps the photogenerated electron of TiO_2 and reduces the electron-hole recombination time of TiO_2. Although a number of methods have been developed for the incorporation of TiO_2 in silica spheres including gas phase synthesis [21], dry coating synthesis [22], sol-gel process [23, 24], and microemulsion method [25], the above methods have the disadvantages including impurities, high cost, long time to encapsulate TiO_2, multistep coating process, and complicated experimental procedure.

Ultrasound is a promising technology whose applications have been rapidly growing due to its unique effects compared to the conventional agitation, such as rapid volumetric heating, increased reaction rates and shortened reaction time, enhanced reaction selectivity, and energy saving [26]. In addition, in many cases, reactions under ultrasound irradiation represent environmentally friendly processes, using small amounts of solvents and consuming less energy [27]. Furthermore, ultrasonic irradiation provides minimal side reactions [28]. In this study, we report a fast, simple, and low temperature ultrasonic method to synthesize SiO_2@TiO_2 core-shell nanocomposite particles.

2. Experimental

2.1. Materials. The precursors used for the preparation of SiO_2 and TiO_2 were tetraethoxysilane (TEOS), ethanol (99.5%, KANTO Chemical Co., Japan), and titanium-tetra-n-butoxide (TBOT, Sigma-Aldrich) solutions. Ammonium hydroxide (NH_4OH) was purchased from WAKO Pure Chemical Industries Ltd., Japan. Degussa P-25 was used as commercial pure TiO_2 in all the experiments. All other reagents were of analytical grade and were used in experiments without further purification. Milli-Q water with a resistivity of 18.3 MΩ cm was used in all the preparations.

2.2. Synthesis of Silica Nanoparticles. The ultrasound synthesis of silica powders was performed using an ultrasound instrument (20 kHz, 700W; Q 700, QSONIC, USA). To 20 mL ethanol solution of TEOS, the desired amount of water and ammonium hydroxide were added under magnetic stirring so that the concentrations of TEOS, H_2O, and NH_4OH were 0.22 M, 6 M, and 2 M, respectively. Immediately, the mixture was then ultrasound irradiated at room temperature for 1 hr. After the synthesis, the resulting silica spheres were separated by centrifugation and washed with ethanol and water. Finally, the prepared silica powder, SiO_2(s), was dried at 60°C for 24 hrs.

2.3. Preparation of SiO_2@TiO_2 Core-Shell Nanocomposite Particles. The coating reaction was performed in ethanol at room temperature by the hydrolysis and condensation of titanium-tetra-n-butoxide (TBOT). At first, dispersion of SiO_2 nanoparticles in ethanol was performed by sonication. Typically, 0.40 g of prepared SiO_2 nanoparticles was taken in a 100 mL Pyrex beaker, and then, 20 mL of ethanol was added into it. The mixture was then ultrasonicated for 5 min to ensure good dispersion of the SiO_2 nanoparticles. After that, an appropriate amount of TBOT (1.5×10^{-3} mol to 9.0×10^{-3} mol), ammonia (to maintain the concentration of 0.8 M), water (to maintain the concentration of 11 M), and ethanol was added into the dispersion. The mixture was exposed to high intensity ultrasound irradiation with a Ti probe having a diameter of 6 mm and an amplitude of 120 μm for 2 hrs. The probe was inserted to an optimum depth of the reaction mixture during the experiment. The ultrasound equipment produces acoustic waves at a frequency of

20 kHz. After ultrasonic irradiation, the resulting suspensions were centrifuged at 4000 rpm for 10 min and washed with ethanol for three times and water to remove all unreacted reagents. The SiO_2@TiO_2 core-shell nanocomposite particles were then dried at 120°C for 5 h. The prepared sample names are denoted as SiO_2-TiO_2-1, SiO_2-TiO_2-2, SiO_2-TiO_2-3, SiO_2-TiO_2-4, and SiO_2-TiO_2-5 for 1.5×10^{-3} mol, 3.0×10^{-3} mol, 4.5×10^{-3} mol, 6.0×10^{-3} mol, and 9.0×10^{-3} mol of TBOT loading, respectively.

2.4. Material Characterization. The morphological structure of the samples was investigated by field emission scanning electron microscopy (FE-SEM) using S-4500 (Hitachi Ltd., Japan) and transmission electron microscopy (TEM) using JEM-2010 (JEOL Ltd., Japan). FE-SEM observation was performed at an accelerating voltage of 5 kV and current of 10 μA. Prior to the observation, the powder was dropped onto carbon tape. Then, samples were coated with a few nanometers of platinum using a Pt-Pd ion coater (Hitachi, E-1030, Japan). For TEM measurement, powder specimens were suspended in ethanol, and an aliquot of 50 μL was deposited on a copper grid coated with a holey carbon film. The copper grids were allowed to dry at room temperature in air.

X-ray photoelectron spectroscopy (XPS) measurements were performed using PHI 5000 Versa Probe-II (ULVAC-PHI Inc., Japan) by dropping the powder samples on the carbon tape using Mg Kα X-ray source operating at 200 W (15 kV). The vacuum level in the main chamber was under 1×10^{-7} Pa. The emission angle of the specimen from the surface normal was 45°. A wide scan (binding energy range: 0-900 eV, pass energy: 187.85 eV) was performed to detect all types of element on the surface, and narrow scan was performed for each element, C 1s, Si 2p, O 1s, Ti $2p_{2/3}$, and Ti $2p_{1/2}$, with the pass energy of 58.7 eV. The adventitious C 1s peak at 284.8 eV was used as reference for all binding energies.

FT-IR spectra were carried out using a system (FT/IR-4100 spectrometer, Jasco Corp., Japan) in the range 4000-400 cm^{-1} with a resolution of 2.0 cm^{-1}. Measurements were performed with a KBr pellet containing a small amount of sample powder. The weight ratio between sample powder and KBr was 1 : 10.

The UV-vis spectroscopic measurements were performed with a UV-vis spectrophotometer (V-560, Jasco Corp., Japan) in the wavelength region of 300-700 nm and band width of 5 nm.

A Zeta PALS apparatus (Zetasizer Nano, Malvern Instrument Ltd., Malvern, UK) was used to investigate the electrophoretic behavior of the materials.

X-ray powder diffraction (XRD) spectra were recorded with a powder diffractometer (Ultima IV, Rigaku Corp., Japan) with Cu-Kα radiation.

2.5. Photocatalytic Activity Measurement. The photocatalytic activities of uncoated SiO_2 nanoparticles and SiO_2@TiO_2 core-shell nanocomposite particles were determined by methylene blue (MB) degradation under UV radiation. Photocatalytic experiments were performed at 293 K using a 100 mL Pyrex beaker in a reaction chamber (50 cm × 50 cm × 50 cm) containing five bulbs (22 inches, 15 W) with the strongest band at the wavelength of 352 nm. The distance between the UV lamp and the surface of the solution was about 15 cm. The average UVA and UVB intensities of exposure for all measurements were around 80 and 0.25 W/m^2 measured by a UV monitor (MS-211-1, Eiko Instruments Co. Ltd.) with the peak intensity of 352 nm. The details of the experimental procedure were described somewhere else [29]. The initial concentration of the dye was 1.00×10^{-5} M, and different amounts of SiO_2@TiO_2 composite particles were added in the dye solution so that the TiO_2 content in all the composites were 0.1 g. MB solution and photocatalysts were mixed in a beaker and kept at dark for 30 min with magnetic stirring to ensure the adsorption/desorption equilibrium between photocatalyst and dye. After switching on the UV lamp, at each time step, an aliquot of 2 mL of the aqueous suspension was taken from the beaker and centrifuged to separate the photocatalytic particles. The total volume of this mixture was kept constant by adding the same amount of water. The remaining MB dye concentration after irradiation was measured by UV-visible spectroscopy.

3. Results and Discussion

For the preparation of nanomaterials by using ultrasonic irradiation, phenomena responsible for sonochemistry can be characterized into primary sonochemistry, secondary sonochemistry, and physical modifications. It is important to note that the chemical and physical effects of ultrasound do not arise from a direct interaction between chemical species and sound waves but rather from the physical phenomenon of acoustic cavitation, namely, the formation, growth, and implosion of bubbles [30]. The bubbles collapse implosively in less than a microsecond under ultrasonic irradiation and produce intense local heating (~5000 K), high pressures (~1000 atm), and large heating and cooling rates (>109 K/s), in a microscopic region of the sonicated liquid [30, 31]. Furthermore, the implosive collapse of bubbles facilitates the production of intense shock waves and microjetstream in the solutions, which promote the transfer of reactants and prevent the nanoparticles from aggregation [32]. Besides, it could enhance the dissolution processes and promote the chemical reactions and kinetics [24]. In the present study, the cavitation bubbles are filled with ethanol, water, ammonia, and TBOT vapors. Since the vapor pressure of ethanol (bp 78°C) at 32°C is much higher than that of TBOT (bp 312°C), the concentration of TBOT molecules inside the bubble is negligibly low and the ultrasound-driven hydrolysis of TBOT occurs in the liquid reaction zone rather than in the gas phase of the cavitation. The temperature of the hot spot in the vicinity of the collapsing bubble has been estimated to be about several thousand Kelvin. Consequently, transient temperature jumps in the liquid shell surrounding the cavitation bubble would lead to a strong local acceleration of titania nucleation [33].

3.1. SEM Images. The surface morphology of the uncoated SiO_2, pure TiO_2, and SiO_2@TiO_2 core-shell nanocomposite particles was investigated using SEM, and the results are

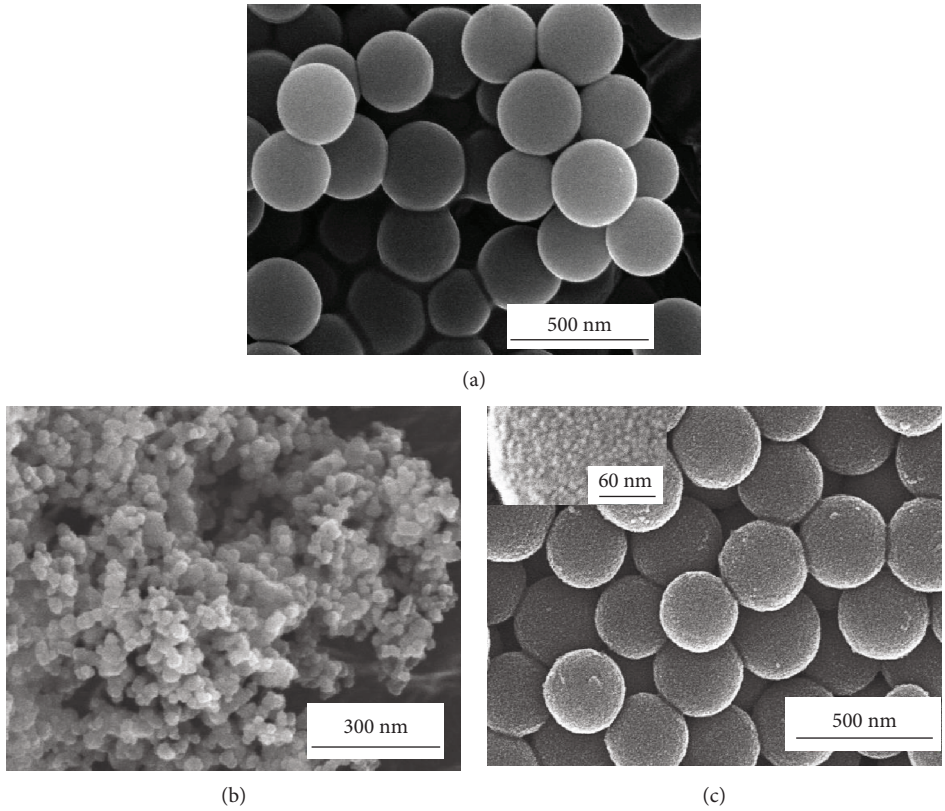

Figure 1: FE-SEM images of (a) uncoated SiO_2 nanoparticles, (b) pure TiO_2 nanoparticles, and (c) SiO_2@TiO_2 core-shell nanocomposite particles (SiO_2-TiO_2-4).

Table 1: Elemental analysis of SiO_2@TiO_2 samples using EDX and XPS analysis.

Sample	TBOT loading (mol)	Elemental analysis from XRF analysis		Elemental analysis from XPS analysis			
		Si	Ti	Si	C	O	Ti
Uncoated SiO_2	—	100		25.4	21.0	53.6	0.00
Uncoated TiO_2			100	0.00	23.8	51.6	24.6
SiO_2-TiO_2-1	1.5×10^{-3}	95.7	4.3	23.5	16.7	55.7	4.1
SiO_2-TiO_2-2	3.0×10^{-3}	90.3	9.7	20.2	14.8	56.2	8.8
SiO_2-TiO_2-3	4.5×10^{-3}	85.7	14.3	15.6	11.6	55.4	15.4
SiO_2-TiO_2-4	6.0×10^{-3}	80.3	19.7	8.7	12.1	59.4	19.8
SiO_2-TiO_2-5	9.0×10^{-3}	71.2	28.8	3.2	12.2	59.8	24.8

shown in Figures 1(a), 1(b), and 1(c), respectively. The particle size of uncoated SiO_2 was around 250 nm. Pure TiO_2 had a particle size of 30–50 nm, whereas the particle size of TiO_2 in SiO_2@TiO_2 core-shell particles was around 6-10 nm (Figure 1(c), inset). The elemental compositions of the prepared materials measured by XRF and XPS techniques are shown in Table 1. It was observed that the amount of titania content increased with an increase in TBOT loading which indicates the thicker titania layer formation with higher TBOT loading.

3.2. TEM Images. Figures 2(a), 2(b), and 2(c) show the TEM images of uncoated SiO_2, pure TiO_2, and SiO_2@TiO_2 core-shell particles, respectively. It can be found from Figure 2(a) that the diameter of the uncoated SiO_2 was about 250 nm. The surface of SiO_2 core-shell nanoparticles was coated with uniform TiO_2 layer, and the particle size of TiO_2 was 6-10 nm, as shown in Figure 2(b). The phase of TiO_2 on the surface of SiO_2 was confirmed by XRD analysis.

3.3. XRD Patterns. The XRD patterns of the uncoated SiO_2, pure TiO_2, and SiO_2@TiO_2 core-shell nanocomposite particles are shown in Figure 3. Before taking the XRD spectra, pure SiO_2, pure TiO_2, and prepared SiO_2@TiO_2 core-shell particles were heated at 500°C for 1 hour in order to improve the crystallinity of the particles. The XRD pattern of SiO_2

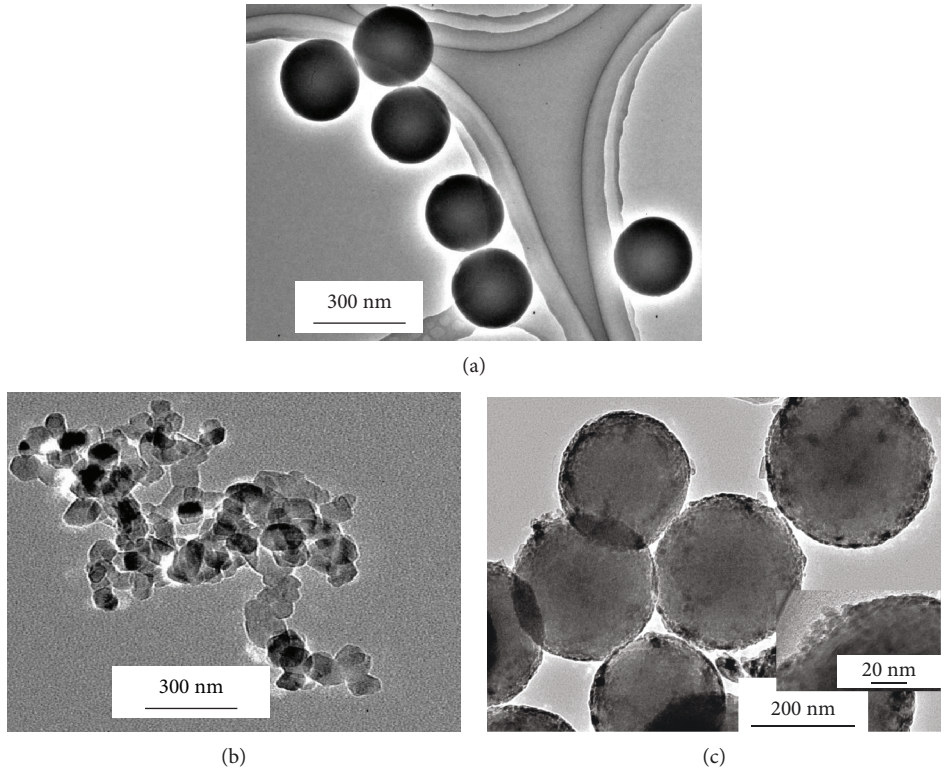

Figure 2: TEM images of (a) uncoated SiO_2 nanoparticles, (b) TiO_2 nanoparticles, and (c) SiO_2@TiO_2 core-shell nanocomposite particles (SiO_2-TiO_2-4).

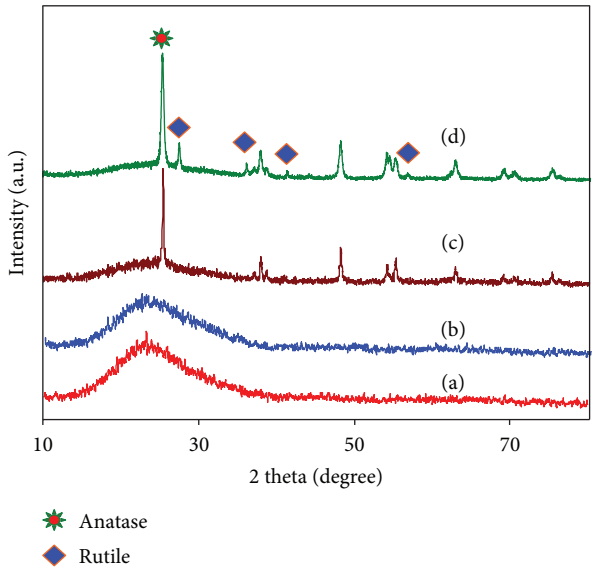

Figure 3: X-ray diffraction patterns of (a) SiO_2 nanoparticles, (b) SiO_2@TiO_2 core-shell nanocomposite particles, SiO_2-TiO_2-4 (as prepared), (c) SiO_2@TiO_2 core-shell nanocomposite particles, SiO_2-TiO_2-4 (annealed at 500°C), and (d) pure TiO_2 nanoparticles.

nanoparticles indicates that the prepared SiO_2 was amorphous in nature. In addition to this, the pure TiO_2 showed peaks that correspond to both the anatase and rutile phases. The prepared SiO_2@TiO_2 core-shell particles did not show any peak that corresponds to TiO_2, which confirms that the crystalline phase of TiO_2 coated on SiO_2 was amorphous. However, after heating the samples at 500°C, the anatase phase of TiO_2 was observed. The absence of a rutile peak in the SiO_2@TiO_2 samples indicates that the prepared nanocomposite particles retained their anatase phase to anatase crystalline phase. It has been established from the literature that the anatase form of titania is very important for the photocatalysis [34, 35].

3.4. XPS Spectra. The presence of TiO_2 coating on SiO_2 nanoparticles was further confirmed from the XPS wide scan spectra of uncoated SiO_2, SiO_2@TiO_2, and pure TiO_2 samples. The XPS wide spectra of the samples as shown in Figure 4 indicate that commercial TiO_2 and SiO_2@TiO_2 samples had Ti 2p peaks whereas no such peak was observed in the case of uncoated SiO_2. In addition, the peak intensities of Ti 2p increased and Si 2p decreased with increasing TBOT loading while the intensity of O 1s remained almost unchanged. The above results indicate successful TiO_2 coating on the surface of SiO_2 particles. The XPS narrow scan spectra of Ti 2p and O 1s are illustrated in Figures 5 and 6, respectively. The spin-coupled Ti ($2p_{3/2}$ and $2p_{1/2}$ peaks) doublet was located at 458.4 and 464.3 eV in pure TiO_2. The shifting of binding energy to higher values in the SiO_2@TiO_2 sample compared to pure TiO_2 is attributed to the formation of Ti-O-Si bonds at the interface of titania coating layer and silica particle surface [36, 37]. Since the electronegativity of Si is higher and polarizability is lower than that of Ti atom, the effective positive charge on Ti atom is increased, electron density around Ti atom is decreased, and the shielding effect is weakened, which results in the increased binding energy. The doublet

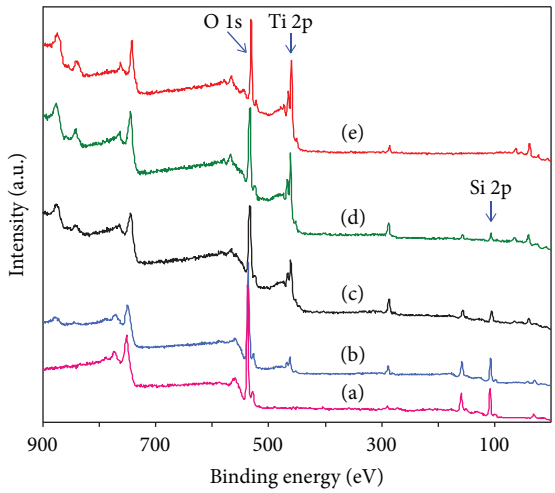

Figure 4: XPS wide scan spectra of (a) SiO_2 nanoparticles, (b) SiO_2-TiO_2-1 (SiO_2@TiO_2 core-shell nanocomposite particles prepared with 1.5×10^{-3} mol TBOT loading), (c) SiO_2-TiO_2-3 (4.5×10^{-3} mol TBOT loading), (d) SiO_2-TiO_2-4 (6.0×10^{-3} mol TBOT loading), and (e) pure TiO_2 nanoparticles.

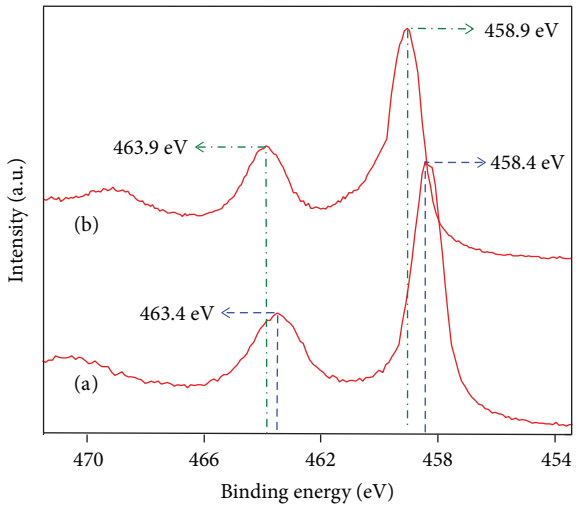

Figure 5: The XPS narrow scan spectra of Ti 2p for (a) pure TiO_2 nanoparticles and (b) SiO_2@TiO_2 core-shell nanocomposite particles, SiO_2-TiO_2-4.

for O 1s peaks was observed at 530.9 eV and 533.4 eV, which corresponds to Ti-O-Ti and Si-O-Si bonds [36, 37], respectively. Compared to the O 1s peak of pure TiO_2 (530.4 eV) (Supplementary Information-1 (SI-1)), the binding energies were shifted towards higher values in SiO_2@TiO_2 core-shell nanocomposites due to the greater electronegativity of Si than that of Ti [36, 37]. From the chemical shift of O 1s and Ti 2p peaks, it can be concluded that SiO_2 nanoparticles were successfully coated with TiO_2 and that Si-O-Ti bond was formed between the interface of SiO_2 and TiO_2.

3.5. UV-vis Absorption Spectra. Figure 7 represents the UV-vis absorption spectra of uncoated SiO_2, SiO_2@TiO_2, and pure TiO_2 samples. Pure TiO_2 showed a peak at 325 nm, SiO_2 nanoparticles did not show any absorption peak, and

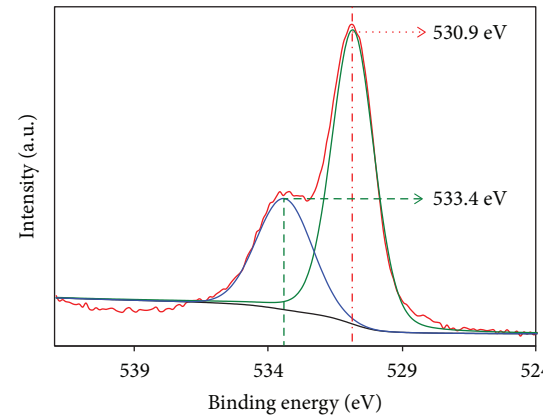

Figure 6: XPS narrow scan spectrum of O 1s of SiO_2@TiO_2 core-shell nanocomposite particles (SiO_2-TiO_2-4).

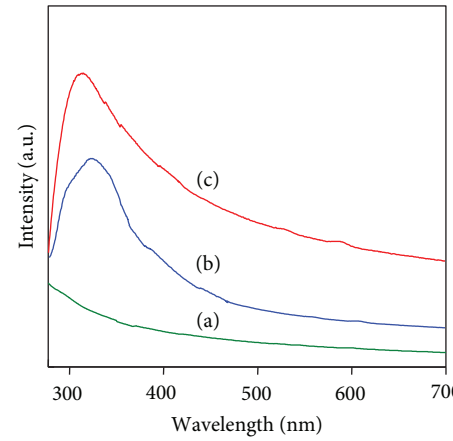

Figure 7: UV-visible absorption spectra of (a) SiO_2 nanoparticles, (b) SiO_2@TiO_2 core-shell nanocomposite particles (SiO_2-TiO_2-4), and (c) pure TiO_2 nanoparticles.

SiO_2@TiO_2 core-shell nanocomposite particles showed a broad peak at 314 nm. It was observed that the absorption maxima of SiO_2@TiO_2 nanoparticles shifted toward the blue region compared to pure TiO_2. This result confirms not only the successful titania coating of SiO_2 particles but also the smaller particle size of TiO_2 in SiO_2@TiO_2 compared to commercial TiO_2 [38]. Therefore, the smaller particle size of TiO_2 in SiO_2@TiO_2 core-shell particles would be beneficial for the photocatalytic reaction as smaller particles provide a more effective surface for organic reactants and light absorption [39].

3.6. FT-IR Spectra. The FT-IR spectra of uncoated SiO_2, SiO_2@TiO_2, and pure TiO_2 are presented in Figure 8. The band at 1105 cm^{-1} was attributed to Si-O-Si asymmetric stretching vibration [40]. The peaks at 800 cm^{-1} and 475 cm^{-1} corresponded to the symmetric stretching and deformation modes of Si-O-Si [40], respectively. A band at around 1450 cm^{-1} was attributed to silanol bonds [41]. The broad band at around 3300 cm^{-1} and 1625 cm^{-1} present in all the samples corresponded to OH stretching and bending of water [42, 43], respectively. Notably, by comparing the

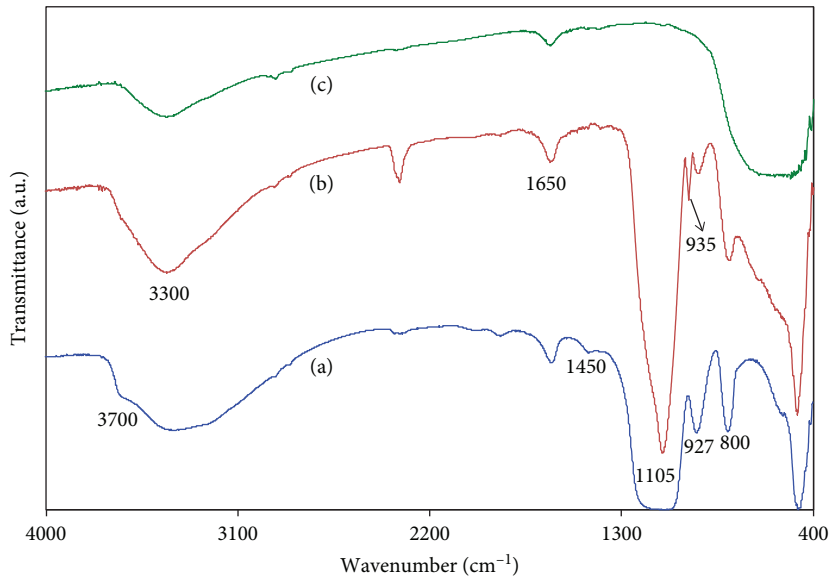

Figure 8: FT-IR spectra of (a) pure SiO_2 nanoparticles, (b) SiO_2@TiO_2 core-shell nanocomposite particles (SiO_2-TiO_2-4), and (c) pure TiO_2 nanoparticles.

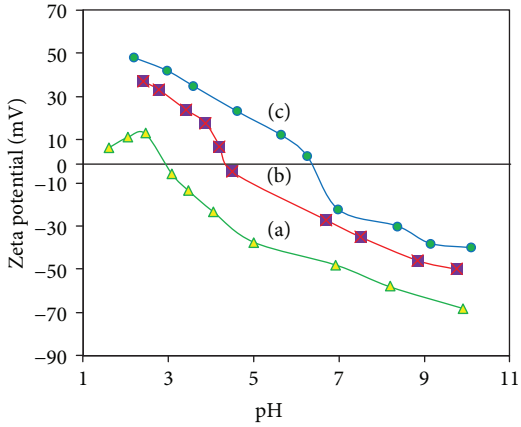

Figure 9: Variation of zeta potential with pH for (a) SiO_2 nanoparticles, (b) SiO_2@TiO_2 core-shell nanocomposite particles (SiO_2-TiO_2-4), and (c) pure TiO_2 nanoparticles.

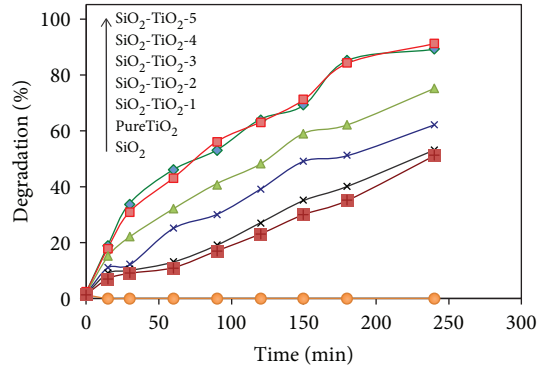

Figure 10: Photocatalytic activities of SiO_2 nanoparticles and SiO_2@TiO_2 core-shell nanocomposite particles prepared with different TBOT loading.

FT-IR spectra of uncoated SiO_2 and TiO_2, the characteristic peak, observed at 935 cm^{-1}, in Figure 8(b), was attributed to Ti-O-Si bond [41, 44]. These FT-IR spectra provided an important information that TiO_2 was successfully coated on SiO_2.

3.7. Zeta Potential Measurement. Zeta potential measurements of the particles were carried out to investigate the presence of TiO_2 coating on the silica surface. The zeta potential values of uncoated SiO_2, pure TiO_2, and SiO_2@TiO_2 core-shell particles are presented in Figure 9. The values of zeta potentials of uncoated SiO_2 changed after TiO_2 coating, which confirms successful TiO_2 coating of SiO_2 particles. Compared to uncoated TiO_2, SiO_2@TiO_2 core-shell nanocomposite particles showed a lowered zeta potential value at neutral pH, which means better dispersion of SiO_2@TiO_2 particles compared to uncoated TiO_2 particles.

4. Photocatalytic Activity Measurement

To evaluate the photocatalytic activity of the SiO_2@TiO_2 core-shell particles and uncoated SiO_2 under UV light irradiation, methylene blue (MB) was chosen as a model pollutant for photocatalytic degradation. The changes in the absorption intensity of MB at 664 nm were monitored by UV-vis spectroscopy. Figure 10 shows the degradation percentages of MB with the photocatalysts. It was found that the uncoated SiO_2 nanoparticles did not show any photocatalytic activity whereas SiO_2@TiO_2 core-shell nanocomposite particles showed better photocatalytic activity compared to uncoated SiO_2 nanoparticles as well as commercial TiO_2. In addition, the photocatalytic activity increases with increasing titania loading. However, the SiO_2-TiO_2-5 (Table 1) sample showed lower photocatalytic activity compared to SiO_2-TiO_2-4 even though the former sample contained higher titania than the latter. The two curves seem, indeed, overlapped, i.e., the behavior seems comparable, which sounds reasonable if

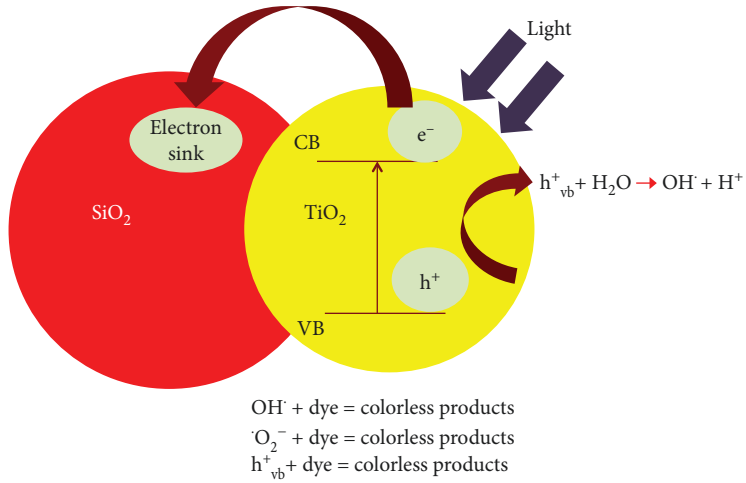

Scheme 1: Scheme of photocatalytic degradation of SiO_2@TiO_2 core-shell nanocomposite particles.

taking into account the fact that the silica nanoparticles are coated at their maximum potential and the titania in excess generates free coreless nanoparticles, which is also confirmed by SEM and TEM images (Supplementary Information-2 (SI-2)).

In general, photocatalytic degradation of dyes is an oxidative process, which involves several active radical formations such as hole (h^+_{VB}), superoxide anion ($^{\cdot}O_2^-$), and hydroxyl radicals ($OH^{\cdot}$). Therefore, when catalysts are illuminated by UV light with photon energy higher than the band gap of TiO_2, electrons (e^-) in the valence band (VB) of TiO_2 excite to its conduction band (CB) with the formation of the same number of holes (h^+_{VB}) left behind in the VB. The various reactions involve in the photocatalytic process can be summarized as follows [45–47]:

$$\begin{aligned}
TiO_2 + h\nu &\rightarrow TiO_2\left(e^-_{CB} + h^+_{VB}\right)\\
h^+_{VB} + OH^-_{(surface)} &\rightarrow OH^{\cdot}\\
h^+_{VB} + H_2O_{(adsorbed)} &\rightarrow OH^{\cdot} + H^+\\
e^-_{CB} + SiO_2 &\rightarrow \text{electron captured by } SiO_2 \text{ surface}\\
e^-_{CB} + O_{2(adsorbed)} &\rightarrow {}^{\cdot}O_2^-\\
{}^{\cdot}O_2^- + H^+ &\rightarrow {}^{\cdot}HO_2\\
{}^{\cdot}HO_2 + {}^{\cdot}HO_2 &\rightarrow {}^{\cdot}OH + OH^- + O_2
\end{aligned} \tag{1}$$

The mechanism of the enhancement of the photocatalytic activity of SiO_2@TiO_2 over pure TiO_2 under UV light irradiation could be illustrated in Scheme 1. In the SiO_2@TiO_2 system, the excited electron transfer from TiO_2 surface to SiO_2 surface and stored temporarily in the silica as it acts as electron sink. Accordingly, the lifetime of the photogenerated pairs is increased. During the photodegradation process, the holes in the valance band react with water and generate $OH^{\cdot}$ radicals and electron stored in the SiO_2 surface produces superoxide anion radicals ($^{\cdot}O_2^-$). Moreover, the insulating character of silica provides the stability of titania particles even at extreme conditions. Furthermore, the formation of the new Ti-O-Si bond in SiO_2@TiO_2 core-shell nanocomposite particles increases the band gap energy of the active center of TiO_2 [20]. As a result, the lifetime of photogenerated electrons (e^-_{CB}), holes (h^+_{VB}), and electrons e^-_{CB} increases which leads to enhanced photocatalytic activity of TiO_2 in SiO_2@TiO_2 samples. Finally, the uniform distribution of titania nanoparticles on the silica sphere surface, as shown in SEM and TEM images (Figures 1(c) and 2(c)), also a good indication of the significant photocatalytic performance of the synthesized nanocomposite particles.

It has also been studied that well-separated particles show better catalytic performance than aggregated particles. Two aggregated catalyst particles compete with each other for the reactants, thus lowering their usage as catalyst particles, while dispersed particles could overcome this drawback. Wu and Lu [48] found that better separation of the immobilized catalyst particles leads to complete utilization of the catalyst particles and thus resulted in the higher rate of photodegradation. The better dispersion of SiO_2@TiO_2 core-shell nanocomposite particles over pure TiO_2 nanoparticles enhances the photocatalytic activity of the catalyst. The catalytic performance of SiO_2@TiO_2 particles was better than uncoated TiO_2 that could also be due to the following reasons: (1) smaller size of TiO_2 in SiO_2@TiO_2 than commercial TiO_2, (2) complete recovery of the catalyst after treatment with low-speed centrifugation, (3) excellent reusing capability, etc. The degradation of MB can be explained by the following elementary mechanism shown in equations (2) and (3). It can involve the direct reaction of the dye with photogenerated holes in the process similar to the photo-Kolbe reaction or oxidation through successive attacks by hydroxyl radicals

$$^{\cdot}O_2^- + MB \rightarrow \text{degradation products} \tag{2}$$

$$OH^{\cdot} + MB \rightarrow \text{degradation products} \tag{3}$$

or superoxide species [49]. The hydroxyl radical in particular is an extremely strong nonselective oxidant that has shown to

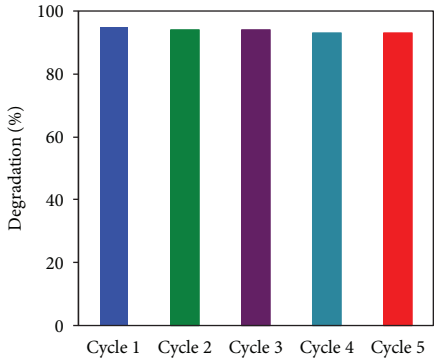

FIGURE 11: Reusability of SiO_2@TiO_2 core-shell photocatalyst (SiO_2-TiO_2-4); pH 7.0; 25°C.

lead to the partial or complete oxidation of many organic chemicals [50].

5. Reusability of SiO_2@TiO_2 Core-Shell Nanocomposite Particles

Photocatalyst stability is one of the most important factors for its practical application. As a consequence of that, the stability and reuse ability of SiO_2@TiO_2 core-shell nanocomposite particles were examined by conducting the photocatalytic experiments with model dye MB under UV irradiation cycled for five times as shown in Figure 11. After each run, SiO_2@TiO_2 particles were recovered by centrifugation at 4000 rpm, washed with deionized water thrice, dried, and reused for the next run. On the other hand, 11000 rpm speed was required to recover the commercial TiO_2 with a particle size of 20-30 nm. The results of the reusing test indicated that there was no considerable difference in the activity of the prepared SiO_2@TiO_2 catalyst at least for five cycles. Thus, the SiO_2@TiO_2 catalyst can be separated after dye treatment with low power centrifugation and reused successfully without loss of activity.

6. Conclusions

We have shown a simple, fast, and environment-friendly ultrasonic irradiation method for the synthesis of SiO_2@TiO_2 core-shell nanocomposite particles using TBOT in SiO_2-ethanol suspension. Compared to the conventional methods, which need long reaction time, the ultrasonic-assisted method allows the formation of TiO_2 nanoparticles on the SiO_2 surface within short reaction time (2 hours). SEM and TEM images revealed that 6–10 nm sized TiO_2 nanoparticles were uniformly coated on the surface of around 250 nm sized SiO_2 nanoparticles. XRD analysis showed that TiO_2 deposited on the surface of the SiO_2 was amorphous, and the anatase crystalline form of TiO_2 was formed after heating the composite materials at 500°C. A new Ti-O-Si bond at the interface between SiO_2 and TiO_2 particles identified by FT-IR and XPS has confirmed the successful TiO_2 coating of SiO_2 nanoparticles. Encapsulation of anatase TiO_2 on high surface area SiO_2 resulted in better photocatalytic ability compared to commercial TiO_2, easy separation, and complete recovery of the catalyst after the dye treatment with low-speed centrifugation (4000 rpm). The prepared nanocomposite particles were reused successfully for five cycles without loss of catalytic activity. The ultrasonic-assisted approach can also be extended for the fabrication of a variety of core-shell nanocomposites such as Au-TiO_2, Ag-TiO_2, ZrO_2-TiO_2, and SnO_2-TiO_2. Research on these issues is currently underway.

Data Availability

The data used to support the findings of this study are included within the article.

Conflicts of Interest

The authors declare that they have no conflicts of interest.

Acknowledgments

This work was financially supported by the Ministry of Science and Technology, Bangladesh, and the University Grant Commission, Bangladesh.

Supplementary Materials

Supplementary Information-1 (SI-1): XPS narrow scan spectra of O 1s of pure TiO_2 revealed that the binding energy of O 1s of pure TiO_2 was 530.1 eV. Supplementary Information-2 (SI-2): SEM and TEM images of TiO_2-coated SiO_2 nanocomposite particles with high titanium-tetra-n-butoxide (TBOT) loading indicated the significant free TiO_2 nanoparticle formation. *(Supplementary Materials)*

References

[1] J. Duarte Baumer, A. Valério, S. M. A. G. U. de Souza, G. S. Erzinger, A. Furigo Jr., and A. A. U. de Souza, "Toxicity of enzymatically decolored textile dyes solution by horseradish peroxidase," *Journal of Hazardous Materials*, vol. 360, pp. 82–88, 2018.

[2] S. Kaviya and E. Prasad, "Correction: Biogenic synthesis of ZnO–Ag nano custard apples for efficient photocatalytic degradation of methylene blue by sunlight irradiation," *RSC Advances*, vol. 5, no. 32, article 25532, 2015.

[3] Y. Badr and M. A. Mahmoud, "Photocatalytic degradation of methyl orange by gold silver nano-core/silica nano-shell," *Journal of Physics and Chemistry of Solids*, vol. 68, no. 3, pp. 413–419, 2007.

[4] Y. Li and K. L. Yeung, "Polymeric catalytic membrane for ozone treatment of DEET in water," *Catalysis Today*, vol. 331, pp. 53–59, 2019.

[5] A. H. Ltaïef, S. Sabatino, F. Proietto et al., "Electrochemical treatment of aqueous solutions of organic pollutants by electro-Fenton with natural heterogeneous catalysts under pressure using Ti/IrO_2-Ta_2O_5 or BDD anodes," *Chemosphere*, vol. 202, pp. 111–118, 2018.

[6] S. N. Singh, *Microbial Degradation of Synthetic Dyes in Wastewaters*, Springer, Cham, Switzerland, 2015.

[7] S. Mozia, M. Tomaszewska, and A. W. Morawski, "Photodegradation of azo dye Acid Red 18 in a quartz labyrinth flow

reactor with immobilized TiO_2 bed," *Dyes and Pigments*, vol. 75, no. 1, pp. 60–66, 2007.

[8] S. Nouren, H. N. Bhatti, M. Iqbal et al., "By-product identification and phytotoxicity of biodegraded direct yellow 4 dye," *Chemosphere*, vol. 169, pp. 474–484, 2017.

[9] U. Pagga and K. Taegr, "Development of a method for adsorption of dyestuffs on activated sludge," *Water Research*, vol. 28, no. 5, pp. 1051–1057, 1994.

[10] M. R. Hoffmann, S. T. Martin, W. Choi, and D. W. Bahnemann, "Environmental applications of semiconductor photocatalysis," *Chemical Reviews*, vol. 95, no. 1, pp. 69–96, 1995.

[11] N. Negishi, Y. Miyazaki, S. Kato, and Y. Yang, "Effect of HCO_3^- concentration in groundwater on TiO_2 photocatalytic water purification," *Applied Catalysis B: Environmental*, vol. 242, pp. 449–459, 2019.

[12] S. Munir, D. D. Dionysiou, S. B. Khan, S. M. Shah, B. Adhikari, and A. Shah, "Development of photocatalysts for selective and efficient organic transformations," *Journal of Photochemistry and Photobiology B: Biology*, vol. 148, pp. 209–222, 2015.

[13] O. Ola and M. M. Maroto-Valer, "Review of material design and reactor engineering on TiO_2 photocatalysis for CO_2 reduction," *Journal of Photochemistry and Photobiology C*, vol. 24, pp. 16–42, 2015.

[14] C. Xu, G. P. Rangaiah, and X. S. Zhao, *Industrial and Engineering Chemistry Research*, vol. 53, no. 38, pp. 14641–14649, 2014.

[15] J. Zhang, X. Jin, X. Yu et al., "An in situ polymerization-encapsulation approach to prepare TiO_2–graphite carbon–Au photocatalysts for efficient photocatalysis," *Particle and Particle Systems Characterization*, vol. 35, article 17002, 2018.

[16] M. Noorjahan, M. Pratap Reddy, V. Durga Kumari, B. Lavédrine, P. Boule, and M. Subrahmanyam, "Photocatalytic degradation of H-acid over a novel TiO_2 thin film fixed bed reactor and in aqueous suspensions," *Journal of Photochemistry and Photobiology A: Chemistry*, vol. 156, no. 1-3, pp. 179–187, 2003.

[17] N. Xu, Z. Shi, Y. Fan, J. Dong, J. Shi, and M. Z.-C. Hu, "Effects of particle size of TiO_2 on photocatalytic degradation of methylene blue in aqueous suspensions," *Industrial and Engineering Chemistry Research*, vol. 38, no. 2, pp. 373–379, 1999.

[18] W. Li and D. Zhao, "Extension of the Stöber method to construct mesoporous SiO_2 and TiO_2 shells for uniform multifunctional core–shell structures," *Advanced Materials*, vol. 25, no. 1, pp. 142–149, 2013.

[19] B. J. Jankiewicz, D. Jamiola, J. Choma, and M. Jaroniec, "Silica–metal core–shell nanostructures," *Advances in Colloid and Interface Science*, vol. 170, no. 1-2, pp. 28–47, 2012.

[20] X. Gao and I. E. Wachs, "Titania–silica as catalysts: molecular structural characteristics and physico-chemical properties," *Catalysis Today*, vol. 51, no. 2, pp. 233–254, 1999.

[21] J. Fitz-Gerald, R. K. Singh, H. Gao, and S. J. Pennycook, "Nanometric dry powder coatings using a novel process," *Kona*, vol. 17, pp. 173–182, 1999.

[22] R. Pfeffer, R. N. Dave, D. Wei, and M. Ramlakhan, "Synthesis of engineered particulates with tailored properties using dry particle coating," *Powder Technology*, vol. 117, no. 1-2, pp. 40–67, 2001.

[23] J. Retuert, R. Quijada, and V. M. Fuenzalida, *Journal of Materials Chemistry*, vol. 10, no. 12, pp. 2818–2822, 2000.

[24] S. Ullah, E. P. Ferreira-Neto, A. A. Pasa et al., "Enhanced photocatalytic properties of core@shell SiO_2@TiO_2 nanoparticles," *Applied Catalysis B: Environmental*, vol. 179, pp. 333–343, 2015.

[25] K. D. Kim and H. T. Kim, "Comparison of the growth mechanism of TiO_2-coated SiO_2 particles prepared by sol–gel process and water-in-oil type microemulsion method," *Colloids and Surfaces A: Physicochemical and Engineering Aspects*, vol. 255, no. 1-3, pp. 131–137, 2005.

[26] H. Zang, Y. Zhang, Y. Zang, and B.-W. Cheng, "An efficient ultrasound-promoted method for the one-pot synthesis of 7,10,11,12-tetrahydrobenzo[c]acridin-8(9H)-one derivatives," *Ultrasonics Sonochemistry*, vol. 17, no. 3, pp. 495–499, 2010.

[27] G. Zbancioc, O. Florea, P. G. Jones, and I. I. Mangalagiu, "An efficient and selective way to new highly functionalized coronands or spiro derivatives using ultrasonic irradiation," *Ultrasonics Sonochemistry*, vol. 19, no. 3, pp. 399–403, 2012.

[28] J. P. Hallett and T. Welton, "Room-temperature ionic liquids: solvents for synthesis and catalysis. 2," *Chemical Reviews*, vol. 111, no. 5, pp. 3508–3576, 2011.

[29] N. M. Bahadur, T. Furusawa, M. Sato, F. Kurayama, and N. Suzuki, "Rapid synthesis, characterization and optical properties of TiO_2 coated ZnO nanocomposite particles by a novel microwave irradiation method," *Materials Research Bulletin*, vol. 45, no. 10, pp. 1383–1388, 2010.

[30] E. Kuna, R. Behling, S. Valange, G. Chatel, and J. C. Colmenares, "Sonocatalysis: a potential sustainable pathway for the valorization of lignocellulosic biomass and derivatives," *Topics in Current Chemistry*, vol. 375, no. 2, p. 41, 2017.

[31] K. S. Suslick, "Sonochemistry," *Science*, vol. 247, no. 4949, pp. 1439–1445, 1990.

[32] R. Ambati and P. R. Gogate, "Ultrasound assisted synthesis of iron doped TiO_2 catalyst," *Ultrasonics Sonochemistry*, vol. 40, pp. 91–100, 2018.

[33] H. Xu, B. W. Zeiger, and K. S. Suslick, "Sonochemical synthesis of nanomaterials," *Chemical Society Reviews*, vol. 42, no. 7, pp. 2555–2567, 2013.

[34] J. L. Montaño-Priede, J. P. Coelho, A. Guerrero-Martínez, O. Peña-Rodríguez, and U. Pal, "Fabrication of monodispersed Au@SiO_2 nanoparticles with highly stable silica layers by ultrasound-assisted Stöber method," *Journal of Physical Chemistry C*, vol. 121, no. 17, pp. 9543–9551, 2017.

[35] B. Ohtani, Y. Ogawa, and S. I. Nishimoto, "Photocatalytic activity of Amorphous–Anatase mixture of Titanium(IV) oxide particles suspended in aqueous solutions," *The Journal of Physical Chemistry B*, vol. 101, no. 19, pp. 3746–3752, 1997.

[36] V. Chhabra, V. Pillai, B. K. Mishra, A. Morrone, and D. O. Shah, "Synthesis, characterization, and properties of microemulsion-mediated nanophase TiO2 particles," *Langmuir*, vol. 11, no. 9, pp. 3307–3311, 1995.

[37] Y. L. Lin, T. J. Wang, and Y. Jin, "Surface characteristics of hydrous silica-coated TiO_2 particles," *Powder Technology*, vol. 123, no. 2-3, pp. 194–198, 2002.

[38] F. Garbassi and L. Balducci, "Preparation and characterization of spherical TiO_2–SiO_2 particles," *Microporous and Mesoporous Materials*, vol. 47, no. 1, pp. 51–59, 2001.

[39] S. Kalele, R. Dey, N. Hebalkar, J. Urban, S. W. Gosavi, and S. K. Kulkarni, "Synthesis and characterization of silica–titania core–shell particles," *Pramana*, vol. 65, no. 5, pp. 787–791, 2005.

[40] Z. Ding, X. Hu, G. Q. Lu, P.-L. Yue, and P. F. Greenfield, "Novel silica gel supported TiO_2 photocatalyst synthesized by CVD method," *Langmuir*, vol. 16, no. 15, pp. 6216–6222, 2000.

[41] K. Y. Jung and S. B. Park, "Enhanced photoactivity of silica-embedded titania particles prepared by sol–gel process for the decomposition of trichloroethylene," *Applied Catalysis B: Environmental*, vol. 25, no. 4, pp. 249–256, 2000.

[42] S. Klein, S. Thorimbert, and W. F. Maier, "Amorphous microporous titania–silica mixed oxides: preparation, characterization, and catalytic redox properties," *Journal of Catalysis*, vol. 163, no. 2, pp. 476–488, 1996.

[43] J. Rubio, J. L. Oteo, M. Villegas, and P. Duran, "Characterization and sintering behaviour of submicrometre titanium dioxide spherical particles obtained by gas-phase hydrolysis of titanium tetrabutoxide," *Journal of Materials Science*, vol. 32, no. 3, pp. 643–652, 1997.

[44] A. Yasumori, H. Shinoda, Y. Kameshima, S. Hayashi, and K. Okada, "Photocatalytic and photoelectrochemical properties of TiO_2-based multiple layer thin film prepared by sol–gel and reactive-sputtering methods," *Journal of Materials Chemistry*, vol. 11, no. 4, pp. 1253–1257, 2001.

[45] D. W. Lee, S. K. Ihm, and K. H. Lee, "Mesostructure control using a titania-coated silica nanosphere framework with extremely high thermal stability," *Chemistry of Materials*, vol. 17, no. 17, pp. 4461–4467, 2005.

[46] B. Subash, B. Krishnakumar, M. Swaminathan, and M. Shanthi, "Highly efficient, solar active, and reusable photocatalyst: Zr-Loaded Ag–ZnO for reactive red 120 dye degradation with synergistic effect and dye-sensitized mechanism," *Langmuir*, vol. 29, no. 3, pp. 939–949, 2013.

[47] N. Pugazhenthiran, S. Murugesan, and S. Anandan, "High surface area Ag-TiO_2 nanotubes for solar/visible-light photocatalytic degradation of ceftiofur sodium," *Journal of Hazardous Materials*, vol. 263, pp. 541–549, 2013.

[48] J. C. Wu and S. Y. Lu, "Patch-distribution effect on diffusion-limited process in dilute suspension of partially active spheres," *The Journal of Chemical Physics*, vol. 124, no. 2, article 024911, 2006.

[49] D. Yang, X. Ni, W. Chen, and Z. Weng, "The observation of photo-Kolbe reaction as a novel pathway to initiate photocatalytic polymerization over oxide semiconductor nanoparticles," *Journal of Photochemistry and Photobiology A: Chemistry*, vol. 195, no. 2-3, pp. 323–329, 2008.

[50] S. R. Sarathy and M. Mohseni, "The impact of UV/H_2O_2 advanced oxidation on molecular size distribution of chromophoric natural organic matter," *Environmental Science & Technology*, vol. 41, no. 24, pp. 8315–8320, 2007.